Photofragment translational spectroscopy of allene, propyne, and propyne-d$_3$ at 193 nm

JASON C. ROBINSON†, NIELS E. SVEUM, SCOTT J. GONCHER and DANIEL M. NEUMARK*

Department of Chemistry, University of California, Berkeley,
California 94720, USA and Chemical Sciences Division,
Lawrence Berkeley National Laboratory, Berkeley,
California 94720, USA

The dissociation dynamics of allene, propyne, and propyne-d$_3$ at 193 nm were investigated with photofragment translational spectroscopy. Products were either photoionized using tunable VUV synchrotron radiation or ionized with electron impact. Product time-of-flight data were obtained to determine centre-of-mass translational energy (P(E$_T$)) distributions, and photoionization efficiency (PIE) curves were measured for the hydrocarbon products. The two major product channels evident from this study are atomic and molecular hydrogen loss, with a H:H$_2$ branching ratio of 90:10, regardless of precursor. The P(E$_T$) distribution for each channel is also largely independent of precursor. Both channels appear to occur following internal conversion to the ground electronic state. The propyne-d$_3$ results show that there is extensive isotopic scrambling prior to H(D) atom loss, and that the H:D product ratio is approximately unity. The PIE curves for H(D) atom loss from allene, propyne, and propyne-d$_3$ indicate that the dominant corresponding C$_3$H$_3$ product is the propargyl radical in all cases. There is some evidence from the PIE curves that the dominant C$_3$H$_2$ products from allene and propyne are propadienylidene (H$_2$CCC:) and propargylene (HCCCH), respectively.

1. Introduction

Photodissociation studies of chemical isomers probe the effects of initiating dynamics from various stable points on the ground state potential energy surface. From these studies, one can determine how the overall dissociation mechanism depends on the initial structure of the isomer, thereby probing the global topology of the ground and excited electronic states of the species under study. Unsaturated hydrocarbons are particularly suitable for experiments of this type, since they generally exist in several isomeric forms and have multiple low-lying electronic states accessible by a single UV photon. UV excitation of these species typically deposits sufficient energy for multiple isomerization and dissociation pathways to be thermodynamically accessible, and detailed photodissociation studies can reveal, among other things, whether scrambling between the two (or more) starting isomers becomes facile at any point during the dynamics. For example, in our laboratory very different primary photochemistry from

the 193 nm photodissociation of two C$_4$H$_6$ isomers, 1,2- and 1,3-butadiene [1,2] have been observed, even though both species dissociate via internal conversion to the ground state surface.

The current study focuses on the 193 nm dissociation of allene (H$_2$C=C=CH$_2$) and propyne (HC≡CCH$_3$), two isomers of C$_3$H$_4$, under collisionless conditions. Propyne-d$_3$ (HC≡CCD$_3$) has been studied to further elucidate the dynamics of the dissociation process. The issues that have been addressed here are the primary product channels following dissociation, the relative importance of these product channels, and the partitioning of available energy following dissociation. In identifying the primary product channels, we aim to discriminate between isomeric photoproducts. This study is a reinvestigation and extension of a previous study of the 193 nm photodissociation of allene and propyne conducted in this laboratory [3].

The UV and VUV photodissociation of allene and propyne has been investigated by several other experimental groups [4–13] while numerous theoretical studies [14–21] have been conducted to characterize the ground and excited states of both isomers. The photodissociation dynamics of allene at 193 nm were studied by Jackson *et al.* [5] with molecular beam photofragment

* Corresponding author. Email: dneumark@berkeley.edu
†Present address: Intel Corporation, 2501NW 229th Avenue, Hillsboro OR 97124, USA

translational spectroscopy (PTS), using electron impact (EI) ionization of the scattered photoproducts. This work showed $C_3H_3 + H$ and $C_3H_2 + H_2$ to be the major primary channels, with an $H:H_2$ branching ratio of 89:11, determined by measurement of the scattered H and H_2 signal, as opposed to the heavier, momentum-matched fragments. The centre-at-mass flame translational energy ($P(E_T)$) distributions showed little kinetic energy release for the H-atom loss channel, while the distribution for H_2 loss peaked around 20 kcal/mol. These results imply a dissociation mechanism in which electronic excitation is followed by rapid internal conversion and statistical dissociation from the allene ground state, with no exit barrier with respect to products for H atom loss, but a nonzero exit barrier for the H_2 loss channel. The C_3H_3 product was reasonably assumed to be the propargyl (H_2CCCH) radical. The identity of the C_3H_2 radical was less clear, but it was proposed to be the propadienylidene (H_2CCC) structure formed by 1,1-H_2 elimination from a terminal C atom.

Using 118 nm light to ionize reaction products, Ni *et al.* [8] also found H atom loss to be by far the dominant channel in the 193 nm dissociation of allene. In addition to H_2 loss, they detected signal suggesting a very small amount of $CH_2 + C_2H_2$ production. The structural assignments of C_3H_3 being formed as propargyl radical and C_3H_2 being formed as propadienylidene were supported by more recent work in our laboratory [3] in which allene was photodissociated at 193 nm, and the scattered products were photoionized by tunable vacuum ultraviolet (VUV) synchrotron radiation; the appearance energies for the C_3H_3 and C_3H_2 products were in good agreement with the known ionization potentials of the propargyl [22] and propadienylidene [23] radicals. The $H:H_2$ branching ratio and $P(E_T)$ distribution for the H_2 channel reported in the photoionization study differed from those reported by Jackson [5]. Based on the work presented here, the earlier results appear to be correct.

A theoretical treatment of the allene (and propyne) ground and excited states by Mebel and co-workers [20, 21] supported the overall mechanism invoked to explain the experimental results. They assigned the 193 nm excitation as a vibronically allowed transition to the $^1B_1$ state (in D_{2d}) symmetry and demonstrated how distortion of the nuclear framework in the upper state leads to a crossing between the excited and ground states, thereby providing a reasonably facile pathway for internal conversion. The energetics from these calculations are summarized in figure 1. The dotted lines show the calculated energetics for H and H_2 loss from allene. The H_2 loss channel is less endothermic by 4 kcal/mol, but it has a 9 kcal/mole barrier with respect to products corresponding to the three-centre transition state for 1,1-H_2 elimination, consistent with the lower yield for this channel and its $P(E_T)$ distribution. Figure 1 also illustrates the highest barrier along the allene-propyne isomerization pathway (referenced to propyne), as calculated at the G2(B3LYP) level of theory by Davis *et al.* [24], is included as a dashed line. In fact, this
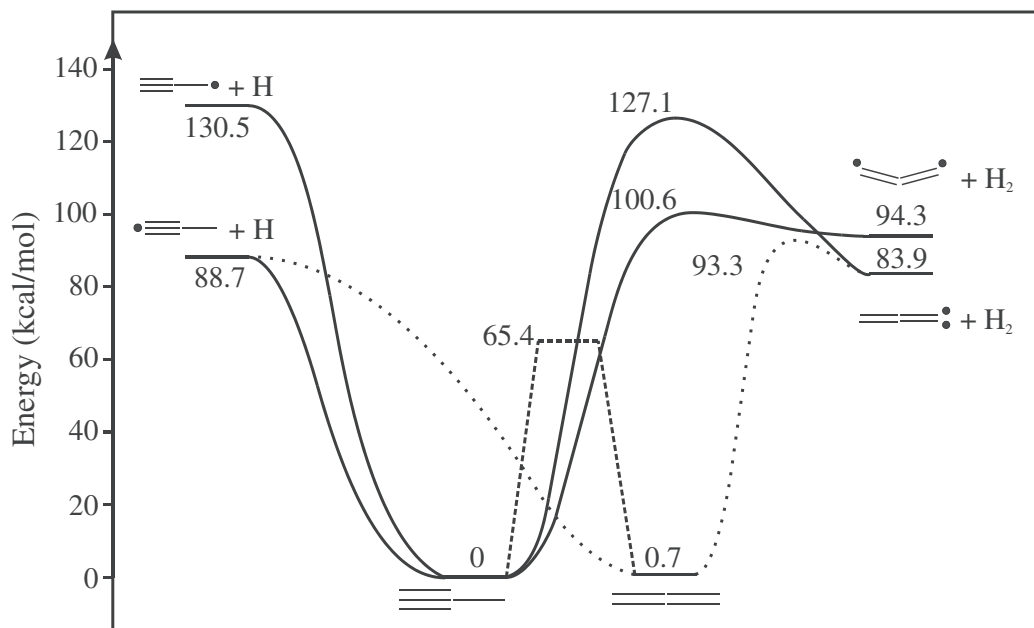
Figure 1. Energy level diagram for allene and propyne dissociation following 193 nm excitation. ●●● radical sites; —— pathways for propyne decomposition, - - - pathways for allene decomposition. All values were taken from theoretical work as described in the text.

pathway is quite complex [18, 24, 25] and involves passage through cyclopropene as an intermediate.

The photodissociation dynamics of propyne are more complex, because cleavage of the inequivalent methyl and acetylenic C–H bonds can occur, resulting in production of the propargyl and propynyl (CH_3CC) radicals, respectively. As shown in figure 1, the acetylenic C–H bond is stronger by 42 kcal/mol, so cleavage of this bond is likely only as a result of excited state dynamics; if internal conversion to the ground state were to occur prior to dissociation, then production of the lower energy propargyl fragment would be strongly favoured. Moreover, once on the ground state, the competition between bond cleavage and isomerization between propyne and allene presents an additional dynamical issue.

The experimental record on C–H bond cleavage from propyne dissociation is somewhat mixed. Bersohn [4] studied the photodissociation of CH_3CCD at 193 nm by monitoring laser-induced fluorescence (LIF) from H and D photolysis products. In this study, no LIF signal from H atoms was detected, suggesting that the C–D bond breaks preferentially. Sun *et al.* [3] found differing photoionization efficiency (PIE) curves for the C_3H_3 products from the photodissociation of propyne and allene at 193 nm; this finding was interpreted to indicate that the C_3H_3 product from propyne was the propynyl radical, in agreement with Bersohn's results. In contrast, Qadiri *et al.* [12, 13] found that the H atom translational energy distributions from propyne photolysis at 193.3, 203.3, 209.0, and 213.3 nm were identical to those from allene, suggesting production of the propargyl radical from each C_3H_4 isomer. Furthermore, Chen *et al.* [11] investigated CD_3CCH by vibrationally exciting the molecule with three quanta of the C–H stretch prior to dissociation at 243.1 nm. Even though the C–H bond was pre-excited, C–D bond fission was found to be the dominant channel, with a reported branching ratio for D loss/H loss of 2.0 ± 0.5. At 157 nm excitation [10], there is evidence for excited state dissociation of the acetylenic bond, along with low energy products attributed to statistical decay on the ground state.

Propyne can also undergo H_2 loss when excited at 193 nm. Ni *et al.* [8] found this to be a minor (<10%) channel, while Sun *et al.* [3] found the H:H_2 branching ratio to be 56:44. However, as was the case with allene, the latter study appears to have overestimated the H_2 loss channel. The mechanism for H_2 loss is strongly coupled to that for H atom loss; if acetylenic C–H bond dissociation dominates, which can only occur on an excited state surface, then H_2 loss must also occur on an excited surface, but if the H atom loss channel corresponds to propargyl formation from ground state dissociation, then H_2 loss also most likely occurs on the

ground state. Figure 1 shows that if H_2 elimination from propyne does occur on the ground state, it can occur via 1,1-H loss to form singlet propargylene (HCCCH), or by 1,3-H loss to form propadienylidene. Although the latter channel is lower in energy, the five-centre transition state for 1,3-H loss is considerably higher in energy than the three-centre TS for 1,1-H loss, so singlet propargylene should be the favoured C_3H_2 isomer from propyne [21]. On the other hand, any isomerization to allene prior to H_2 loss would result in propadienylidene production.

The experiments reported in this paper on allene, propyne, and propyne-d₃ were undertaken in order to gain a fuller understanding of the 193 nm photodissociation dynamics of propyne and to re-investigate some of the claims made in the earlier paper from our group on allene and propyne dissociation [3]. The work reported here comprises new experiments carried out using a molecular beam instrument on the Chemical Dynamics Beamline at the Advanced Light Source (ALS) at the Lawrence Berkeley National Laboratory, in which tunable VUV synchrotron radiation is used to photoionize the fragments, supplemented by experiments on a molecular beam instrument based on electron impact (EI) ionization. The photoionization (PI)-based instrument enables one to greatly reduce the extensive dissociative ionization associated with electron impact. In addition, measuring the photoionization efficiency yield for a particular fragment as a function of VUV energy should allow one to discriminate between isomeric photofragments based on ionization potential. On the other hand, EI cross-sections well above threshold are more available than near-threshold PI cross sections, particularly for open-shell species, facilitating branching ratio measurements on the EI instrument. This capability was particularly useful in measuring the H:H_2 loss ratios from allene and propyne and the H:D branching ratio from the photodissociation of propyne-d₃.

To understand the primary dynamics of the two reaction channels, $P(E_T)$ distributions were determined using photofragment translational spectroscopy. Additionally, PIE curves were measured for the C_3H_3 and C_3H_2 fragments, as well as their deuterated analogues. The $P(E_T)$ distributions for H and D atom loss from allene, propyne, and propyne-d₃ all peak at very low translational energy ($\leqslant 5$ kcal/mol), while those for H_2, HD, and D_2 loss peak at 17–20 kcal/mol. The H:H_2 loss ratios were found to be about 9:1 for both allene and propyne. The H:D branching ratio for photodissociation of propyne-d₃ was nearly unity, indicating extensive isotopic scrambling prior to H(D) atom loss. The PIE curves for H(D) atom loss are essentially the same starting from allene, propyne, or

propyne-d_3, and indicate that the propargyl radical is the dominant C_3H_3 product with no significant propynyl formation, in contrast to our earlier report. The PIE curves for the C_3H_2 product from allene and propyne were slightly different, suggesting identification of the preferred H_2 loss product as propadienylidene from allene and propargylene from propyne, while the PIE curves for the C_3HD and C_3D_2 products from propyne-d_3 were essentially the same.

Our data suggest that the overall photodissociation dynamics comprise internal conversion to the ground state followed by isomerization and dissociation. There are relatively small differences between the photodissociation dynamics of allene and propyne. We consider whether this result reflects similar potential energy topologies for H and H_2 loss from the two precursors, or if instead isomerization between the allene and propyne minima on the global potential energy surface is sufficiently rapid to yield indistinguishable photodissociation dynamics for the two molecules.

2. Experiment

2.1 *PI instrument*

The PI-based apparatus employed in this experiment has been described previously [26, 27]. Briefly, a pulsed photolysis beam crosses a pulsed molecular beam in a rotating source/fixed detector configuration. Scattered photofragments are photoionized by VUV undulator radiation from the ALS after entry into a multiply-differentially pumped detection region. These ions are mass-selected prior to detection. The photofragment time-of-flight (TOF) distribution can be determined at a fixed scattering angle and VUV wavelength, or the mass-selected ion yield can be measured as a function of VUV wavelength to determine the photoionization efficiency curve for a particular fragment.

A pulsed molecular beam of either 6% allene in helium or 5% propyne in helium was generated with a pulsed valve operating at 100 Hz with $\sim$200–400 Torr stagnation pressure, which was maintained using a vacuum regulator. The pulsed valve, which had a 0.5 mm diameter nozzle, was heated to $\sim$80°C to minimize the presence of dimers. A beam of $\sim$5% propyne-d_3 in helium was generated using $\sim$220 Torr stagnation pressure. Propyne (98%) was obtained from Aldrich, allene was obtained from Matheson, and propyne-d_3 (99+%) was obtained from C/D/N Isotopes. All three chemicals were used without further purification. Typically, the section of the initial parent beam that was intersected by the laser was characterized as having a flow velocity $V_0 = 1310$ m/s and a speed ratio $S = 10$ for allene, $V_0 = 1450$ m/s and $S = 11$ for propyne,

$V_0 = 1570$ m/s and $S = 10$ for propyne-d_3. Experiments were also performed on propyne-d_3 seeded in Ne, for which $V_0 = 915$ m/s and $S = 9$.

The molecular beam was skimmed either once or twice and crossed with 193 nm light emitted by a Lambda Physik LPX-200 or COMPex 110 ArF excimer laser. The laser pulse, with a typical energy of 18 mJ, was focused to a 2×4 mm rectangle. The laser beam was perpendicular to both the molecular beam and detector axes, and the molecular beam source could be rotated about the laser beam with respect to the fixed detector. Laser power was controlled to ensure that the TOF spectra were not the result of multiphoton processes. Shot-to-shot background subtraction was employed for spectra taken with photoionization energies above the appearance potential of the species of interest from the parent molecule, but in general, background subtraction was unnecessary given that the ionization energy was maintained below the threshold for the appearance of daughter fragments.

Following dissociation, the neutral photofragments travelled 15.1 cm from the interaction region to the ionization region. Tunable VUV undulator radiation from the Chemical Dynamics Beamline at the ALS was used to ionize the scattered neutral photofragments, and the ionized fragments were mass selected by a quadrupole mass filter. The signal from the fragments of interest was counted as a function of time by a computer-interfaced multichannel scaler (MCS). The ion flight constant (IFC) for the detector was 5.26 μs amu$^{-1/2}$ for the allene and propyne measurements, and it was 5.54 μs amu$^{-1/2}$ or 5.77 μs amu$^{-1/2}$ for the propyne-d_3 measurements (the IFC was confirmed prior to running at the ALS; several separate runs were required). An MCS bin width of 2 μs was used for all allene and propyne spectra presented here, while an MCS bin width of 1 μs was used for propyne-d_3 product TOF spectra; some propyne-d_3 product TOF spectra were rebinned to 3 μs bin widths.

The properties of the VUV undulator radiation used in these experiments have been described in detail [28, 29]. All measurements were conducted at 1.9 GeV electron beam energy, where the low end of the useable VUV radiation range is below 8 eV. The bandwidth of the radiation from the undulator is approximately 2.3%. The higher harmonics of the undulator radiation are removed by a differentially pumped gas filter [30]. In these experiments, the gas filter was maintained at $\sim$25–30 Torr of continuously flowing argon for product TOF measurements. While the upstream mirrors and the gas filter remove the higher harmonics of the undulator radiation, a small blue tail remains on the fundamental. To reduce the effects of this component of the radiation, an MgF_2 window, which transmits no light above

11.2 eV, could be inserted into the path of the undulator radiation. A VUV calorimeter was employed to continuously monitor the VUV radiation flux.

Angle-resolved TOF profiles were obtained by selecting the mass-to-charge ratio (m/e) for the ion of interest, fixing the source angle, and setting the undulator gap to deliver the appropriate photoionization energy. The source angle was changed and more spectra were taken to get a set of spectra for each m/e. PIE curves for specific photofragments were obtained by selecting m/e, fixing the source angle, and scanning the undulator photon energy. In constructing the curve, the scattering signal for each fragment was integrated, background subtracted, and normalized.

2.2 EI instrument

A fixed-source, rotating-detector apparatus based on EI detection was used for additional photodissociation experiments [2, 31]. In general, operating conditions were similar to those described above. A pulsed molecular beam (with a nozzle heated to $\sim 90^\circ$C) of $\sim 5\%$ allene, propyne, or propyne-d₃ in helium was crossed orthogonally with 193 nm light emitted by a Lambda Physik LPX-220i ArF excimer laser. The 12 mJ laser pulse was focused to a 2×4 mm rectangle. The detector could be rotated in the plane defined by the molecular beam and the laser beam. Shot-to-shot background subtraction was used to remove the contribution from the parent molecular beam from the TOF spectra. The neutral photofragments traveled 20.8 cm prior to ionization with ~ 180 eV electrons. The ionized fragments were mass selected by a quadrupole mass filter, and the signal from the fragments of interest was counted as a function of time by a computer-interfaced MCS. The ion flight constant for the detector was $4.9\,\mu\text{s}\,\text{amu}^{-1/2}$. An MCS bin width of 1 µs rebinned to 3 µs was used for the spectra presented here.

3. Results

3.1 PI TOF spectra

Product TOF spectra from allene dissociation were collected for ions with $m/e = 39$ ($C_3H_3^+$), 38 ($C_3H_2^+$), 26 ($C_2H_2^+$), and 14 ($C_2H_2^+$); TOF spectra from propyne dissociation were collected for ions with $m/e = 39$, 38, 26, 25, 15, and 14. Only the TOF spectra for $m/e = 39$ and 38 showed clear evidence for primary dissociation channels, corresponding to the reactions

$$C_3H_4 + h\nu \rightarrow C_3H_3 + H \qquad (R1)$$
$$C_3H_4 + h\nu \rightarrow C_3H_2 + H_2 \qquad (R2)$$
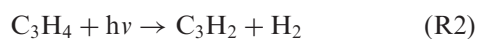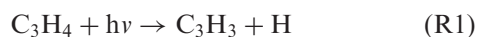
TOF spectra for $m/e = 39$ and 38 were taken at several laboratory angles. None of the lighter masses that were probed showed appreciable signal that would have supported other dissociation pathways. To check for the presence of dimers in the molecular beam, TOF spectra at $m/e = 40$ were collected at a source angle of $\Theta_{\text{LAB}} = 7^\circ$. However, no noticeable signal was detected.

For allene, $m/e = 39$ TOF spectra were collected at $\Theta_{\text{LAB}} = 7^\circ$, 10°, 12°, and 18°, and $m/e = 38$ TOF spectra were collected at $\Theta_{\text{LAB}} = 10^\circ$, 15°, and 20°. For propyne, $m/e = 39$ TOF spectra were collected at $\Theta_{\text{LAB}} = 5^\circ$, 7°, 10°, 12°, and 15°, and $m/e = 38$ TOF spectra were collected at $\Theta_{\text{LAB}} = 8^\circ$, 10°, 15°, and 20°. By selecting multiple undulator settings for different scans, a series of TOF spectra at different VUV photon energies were generated. Figure 2 shows TOF spectra for mass 39 photoproducts from allene at $\Theta_{\text{LAB}} = 7^\circ$ and 10° and propyne at $\Theta_{\text{LAB}} = 7^\circ$ at two different photon energies, 9.9 and 11.4 eV, chosen to lie below and above the onset for ionization of the propynyl radical (see below). The MgF₂ window was used at 9.9 eV but not at 11.4 eV. The TOF spectra at the two photon energies are essentially identical; the implications of this observation are discussed below. Figure 3 shows mass 38 photoproduct TOF spectra for allene and propyne at $\Theta_{\text{LAB}} = 10^\circ$ and 20°, at a photon energy of 11.7 eV.

For propyne-d₃ measurements, TOF spectra were collected for ions with $m/e = 43$, 42, 41, 40, and 39. Each channel of interest leads to primary products with different masses, i.e. $42 + 1$, $41 + 2$, $40 + 3$, and $39 + 4$ correspond to H, D, HD, and D₂ loss, respectively, and primary products from all four channels were detected. For the helium-seeded beam, TOF spectra for $m/e = 42$ and 41 were collected at $\Theta_{\text{LAB}} = 5^\circ$, 7°, 10°, 12°, and 15°, while TOF spectra for $m/e = 40$ and 39 were collected at $\Theta_{\text{LAB}} = 7^\circ$, 10°, 15°, 20°, and 25°. For the neon-seeded beam, TOF spectra for $m/e = 42$ and $m/e = 41$ were collected at $\Theta_{\text{LAB}} = 7^\circ$, 10°, and 15°; additional spectra were collected for $m/e = 42$ at $\Theta_{\text{LAB}} = 13^\circ$. Figure 4 presents sample H and D loss ($m/e = 42$ and $m/e = 41$, respectively) TOF spectra for beams of propyne-d₃ seeded in helium at photon energies of 9.5 and 11.5 eV. TOF spectra for HD and D₂ loss ($m/e = 40$ and $m/e = 39$, respectively) are presented in figure 5.

3.2 EI TOF spectra

Product TOF spectra for allene and propyne were collected on the EI instrument for ions with $m/e = 39$–36 and for several smaller masses, at $\Theta_{\text{LAB}} = 7^\circ$, 10°, and 15°. Sample spectra for $m/e = 39$–36 from propyne are shown in figure 6. In contrast to the PI TOF spectra, the
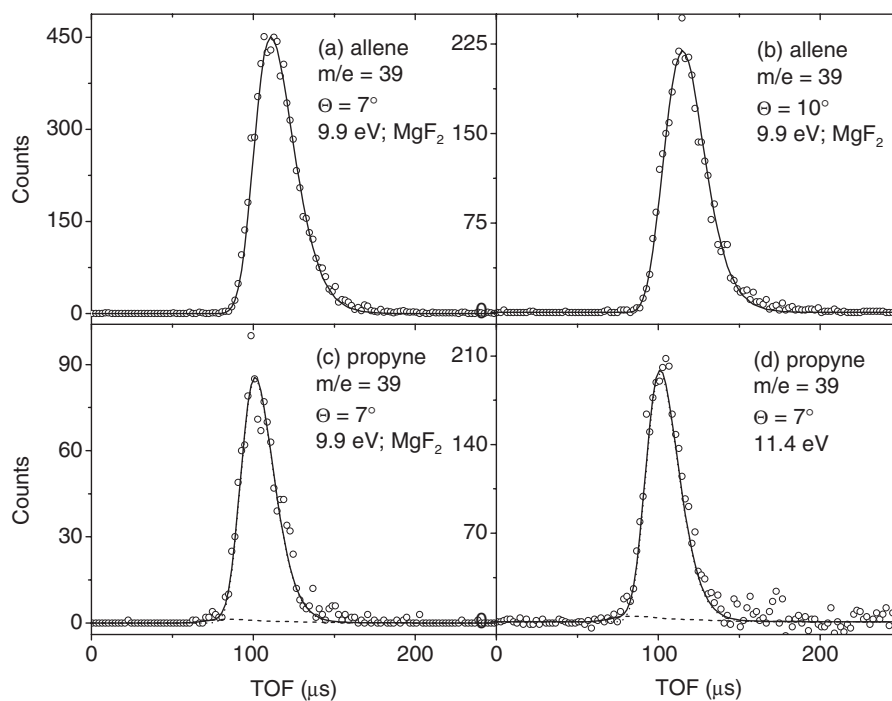
Figure 2. TOF spectra for $m/e = 39$ ($C_3H_3^+$) from allene photodissociation at (a) $\Theta_{LAB} = 7°$ and at (b) $\Theta_{LAB} = 10°$ at a photoionization energy of 9.9 eV; ∘∘∘ data; —— forward convolution fit to the data using the $P(E_T)$ distribution shown in figure 10(a). TOF spectra for $m/e = 39$ ($C_3H_3^+$) from propyne photodissociation at $\Theta_{LAB} = 7°$ using photoionization energies of (c) 9.9 eV and (d) 11.4 eV. ∘∘∘ data; —— total forward convolution fit to the data using the centre-of-mass (CM) translational energy ($P(E_T)$) distribution shown in figure 10(c); - - - contribution from a small amount of dimer dissociation, using the $P(E_T)$ distribution shown in figure 12.
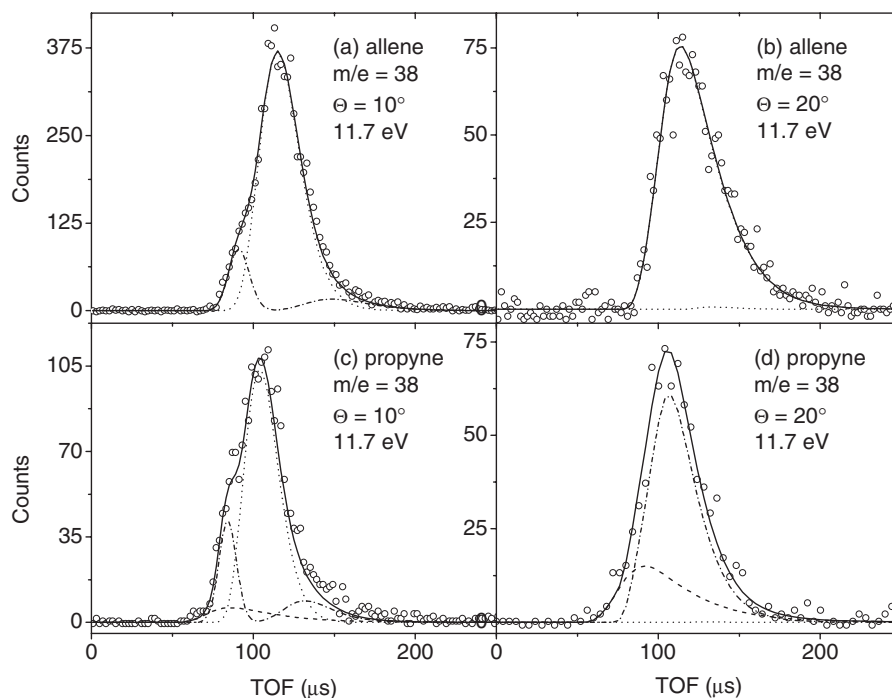
Figure 3. TOF spectra for $m/e = 38$ ($C_3H_3^+$) from allene photodissociation at (a) $\Theta_{LAB} = 10°$ and at (b) $\Theta_{LAB} = 20°$ and from propyne photodissociation at (c) $\Theta_{LAB} = 10°$ and at (d) $\Theta_{LAB} = 20°$. ∘∘∘ data; —— forward convolution fit to the data. ------ fit using the $P(E_T)$ distribution shown in figure 10(b) for allene and figure 10(d) for propyne. ····· fit of a dissociative ionization component from $m/e = 39$ ($C_3H_3^+$) photoproduct. - - - - contribution from dimer dissociation. These two contributions were fitted using the $P(E_T)$ distributions as described in figure 2.
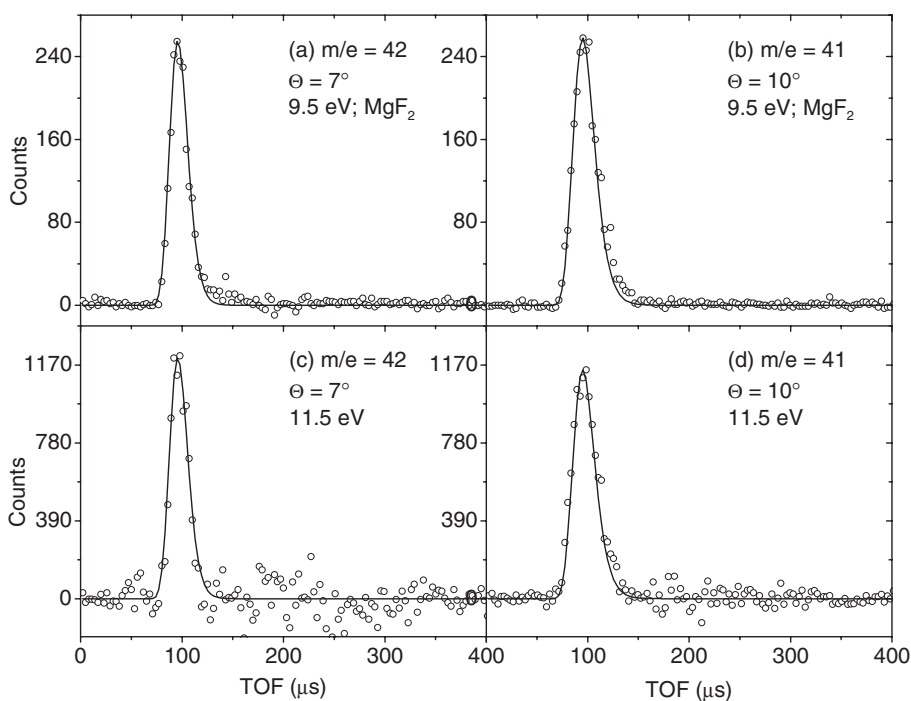
Figure 4. TOF spectra from propyne-d$_3$ photodissociation using 9.5 eV photoionization energy and the MgF$_2$ window at (*a*) $\Theta_{LAB} = 7°$ for $m/e = 42$ (C$_3$D$_3^+$) and (*b*) $\Theta_{LAB} = 10°$ for $m/e = 41$ (C$_3$D$_2$H$^+$). TOF spectra from propyne-d$_3$ photodissociation using 11.5 eV photoionization energy at (*c*) $\Theta_{LAB} = 7°$ for $m/e = 42$ and (*d*) $\Theta_{LAB} = 10°$ for $m/e = 41$. ○○○ data; —— forward convolution fit to the data using the $P(E_T)$ distribution shown in figure 11(*a*) for $m/e = 42$ spectra and the $P(E_T)$ distribution shown in figure 11(*c*) for $m/e = 41$ spectra.
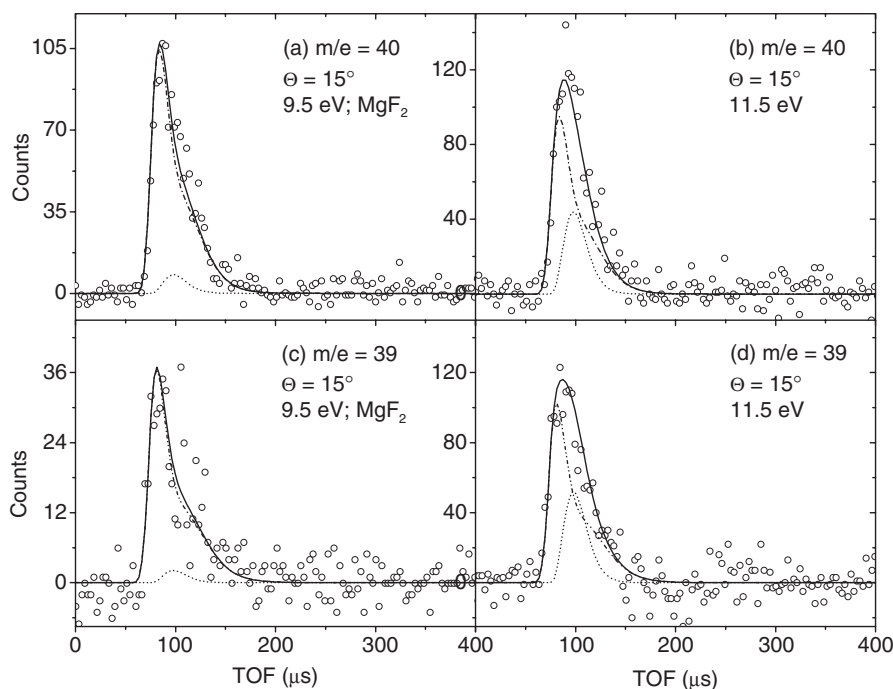
Figure 5. TOF spectra from propyne-d$_3$ photodissociation for $m/e = 40$ (C$_3$D$_2^+$) at $\Theta_{LAB} = 15°$ using (*a*) 9.5 eV and (*b*) 11.5 eV photoionization energy. ○○○ data; —— total forward convolution fit to the data. ------ fit using the $P(E_T)$ distribution shown in figure 11(*b*). TOF spectra from propyne-d$_3$ photodissociation for $m/e = 39$ (C$_3$DH$^+$) at $\Theta_{LAB} = 15°$ using (*c*) 9.5 eV and (*d*) 11.5 eV photoionization energy. ------ forward convolution fit to the data using the $P(E_T)$ distribution shown by a solid line in figure 11(*d*). In all spectra, the short-dashed line represents the fit of dissociative ionization of $m/e = 41$ photoproduct using the $P(E_T)$ distribution shown by a solid line in figure 11(*c*). The MgF$_2$ window was employed for spectra collected at 9.5 eV.
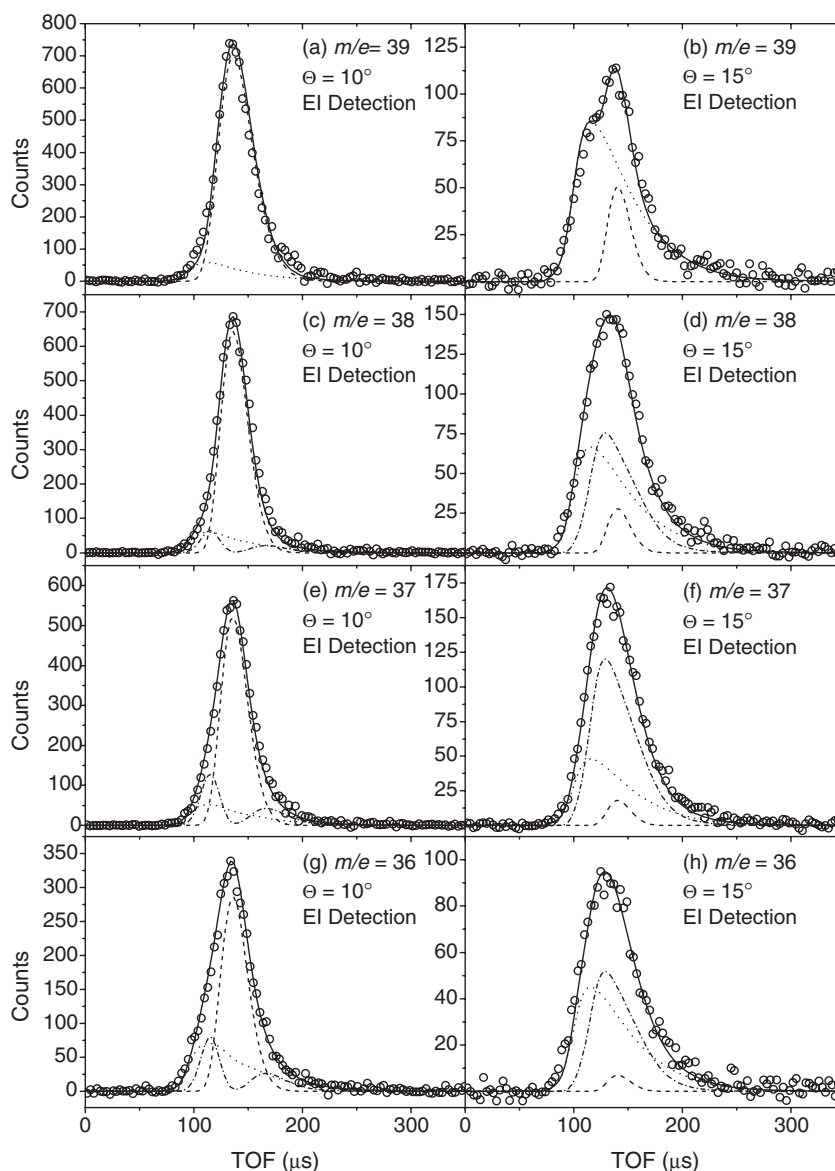
Figure 6. TOF spectra from propyne photodissociation using EI detection at $\Theta_{LAB} = 10°$ and $\Theta_{LAB} = 15°$ for $m/e = 39$ ($C_3H_3^+$) (*a* and *b*), $m/e = 38$ ($C_3H_2^+$) (*c* and *d*), $m/e = 37$ (C_3H^+) (*e* and *f*), and $m/e = 36$ (C_3^+) (*g* and *h*). In all spectra, ∘∘∘ represent the data and —— represents the total forward convolution fit to the data. - - - - represents the contribution from $m/e = 39$ photoproduct using the $P(E_T)$ distribution in figure 10(*c*). ------ represents the contribution from $m/e = 38$ photoproduct using the $P(E_T)$ distribution in figure 10(*d*). · · · · represents the contribution from a small amount of dimer dissociation, using the $P(E_T)$ distribution shown in figure 12.

spectra for $m/e < 39$ have significant contributions from dissociative ionization of the mass 39 C_3H_3 photoproduct, the dominant dissociation channel (see below), particularly at smaller scattering angles. In addition there appears to be a contribution from dissociative ionization of parent dimer in all the TOF spectra. The various contributions to the EI TOF spectra are assessed in section 4.

Product TOF spectra from propyne-d_3 dissociation were collected for ions with $m/e = 42$ and 41 at

$\Theta_{LAB} = 5°$, $7°$, $9°$, $10°$, and $11°$. TOF spectra at $\Theta_{LAB} = 7°$ and $10°$ are shown in figure 7.

3.3 *PIE measurements*

Figure 8 shows PIE curves for the scattered C_3H_3 fragments from allene and propyne dissociation taken at $\Theta_{LAB} = 7°$ with the MgF_2 window in place, as well as PIE curves for C_3H_2 photoproduct at $\Theta_{LAB} = 20°$ without the MgF_2 window. The higher appearance
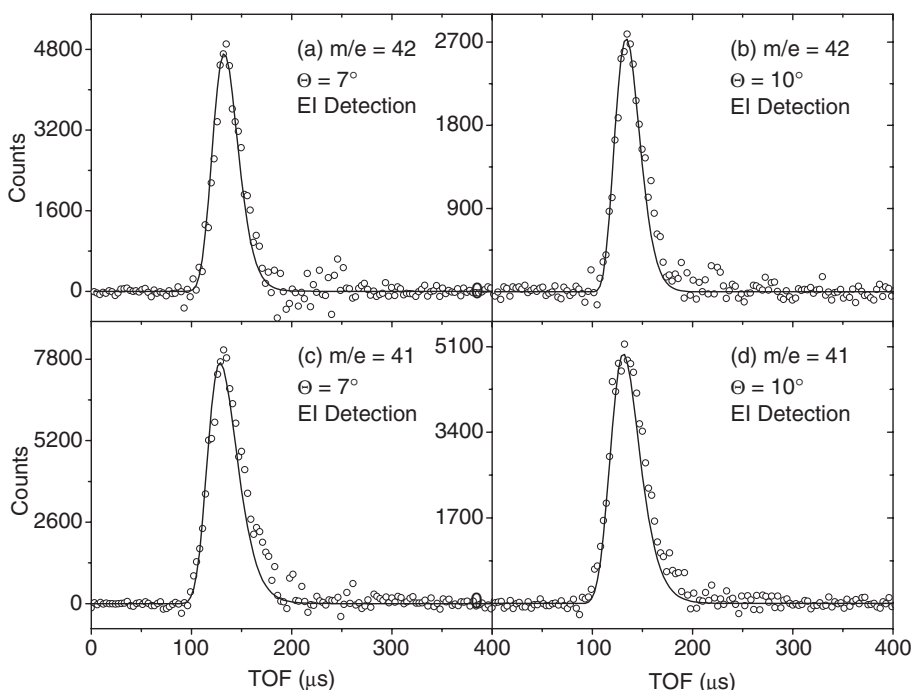
Figure 7. TOF spectra from propyne-d₃ photodissociation using EI detection for $m/e = 42$ ($C_3D_3^+$) at (a) $\Theta_{LAB} = 7°$ and (b) $\Theta_{LAB} = 9°$ and for $m/e = 41$ ($C_3D_2H^+$) at (c) $\Theta_{LAB} = 7°$ and (d) $\Theta_{LAB} = 9°$. ○○○ data; —— forward convolution fit to the data using the $P(E_T)$ distribution shown in figure 11(a) for $m/e = 42$ spectra and the $P(E_T)$ distribution shown in figure 11(c) for $m/e = 41$ spectra.

energy for the $m/e = 38$ products, as evidenced by the PIE spectra in figure 8, necessitates removal of the window, which only transmits light below 11.2 eV. Collection of the data for $m/e = 38$ at $\Theta_{LAB} = 20°$ minimizes the contribution to the PIE curve from dissociative ionization of C_3H_3 product (see section 4.1). For comparison purposes, the PIE curves for fragments with the same m/e from allene and propyne are superimposed in figure 8. Relative scaling of the allene and propyne data was chosen to minimize differences between PIE curves from the two parent species.

The PIE curves show 'tails' that extend to low photon energy, which are characteristic of hot bands from vibrationally excited neutrals. The existence of these tails, combined with the low S/N of the C_3H_2 PIE curves, does not help extraction of accurate IPs from these PIE curves, so only photoionization onsets where the first signal is observed are reported. These onsets are 7.6 ± 0.4 eV for C_3H_3 from allene, $7.6 \pm 0.$ eV for C_3H_3 from propyne, 9.0 ± 0.5 eV for C_3H_2 from allene, and 8.8 ± 0.5 eV for C_3H_2 from propyne. The PIE curves for the C_3H_3 products ($m/e = 39$, figure 8(a)) from allene and propyne are quite similar, in contrast to those reported by our lab previously, [3] which are now believed to be incorrect. The PIE curve for C_3H_2 ($m/e = 38$, figure 8(b)) products from propyne show more intensity below 10 eV than the corresponding

curve from allene, while the allene curve shows more intensity above 10 eV. However, the error bars are larger for these curves because the signal is considerably lower for $m/e = 38$.

Figure 9 presents the PIE curves for fragments produced in the photodissociation of propyne-d₃. The PIE curves for $m/e = 42$ and $m/e = 41$ (H and D loss) are superimposed in figure 9(a), while those for $m/e = 40$ and 39 (HD and D_2 loss) are superimposed in figure 9(b). As in figure 8, relative scaling was chosen to minimize differences between the superimposed curves. There appear to be no significant differences between the superimposed curves in figure 9(a) or 9(b). In figure 9(a), each PIE curve shows a photoionization onset of 8.0 ± 0.4 eV. The PIE curves in figure 9(b) show photoionization onsets of 8.0 ± 0.4 eV for $m/e = 40$ and 8.5 ± 0.4 eV for $m/e = 39$.

3.4 *Electronic structure calculations on the propynyl radical*

Interpretation of the PIE curves for the C_3H_3 fragment for allene and propyne in figure 8 requires knowledge of the ionization potentials (IPs) for the various C_3H_3 isomers. The IP of propargyl has been determined by ZEKE spectroscopy to be 8.763 eV [22], while the IP for the cyclopropenyl radical is reported to be 6.6 eV [32].
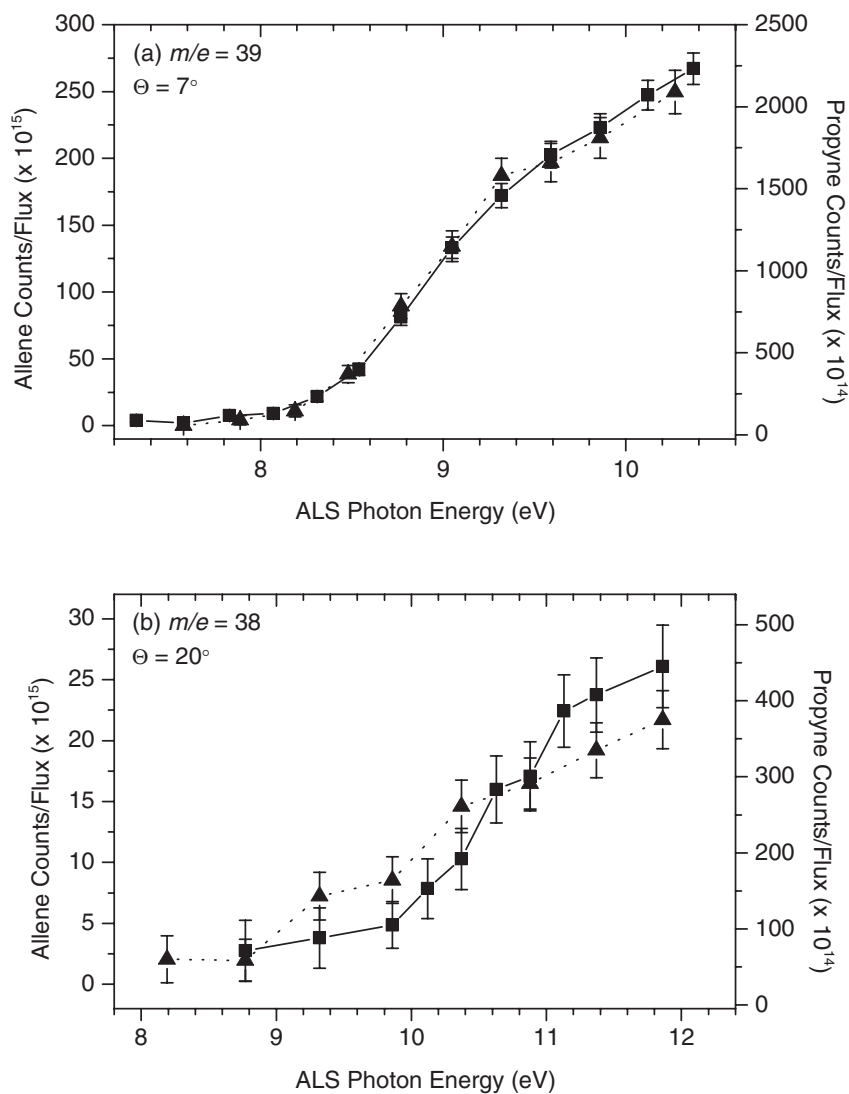
Figure 8. (*a*) Photoionization efficiency curves for $m/e = 39$ ($C_3H_3^+$) photoproduct at $\Theta_{LAB} = 7°$ for allene and propyne photodissociation, using the MgF_2 window for reduction of a residual high-energy tail in the undulator radiation. (*b*) Photoionization efficiency curves for $m/e = 38$ ($C_3H_2^+$) photoproduct at $\Theta_{LAB} = 20°$ for allene and propyne photodissociation, also using the MgF_2 window. The curves are scaled to one another for comparison. The solid squares with a solid line represent the allene data points with 2σ error bars, while the solid triangles with a dashed line represent the propyne data points with 2σ error bars.

The adiabatic and vertical IP's of propargyl are very similar, given that the largest peak in its photoelectron spectrum is the transition to the ionic ground vibrational state [33]. No experimental determination of the ionization potential of the propynyl radical (CH_3CC) has been performed to date. Therefore, electronic structure calculations were performed to determine the vertical IP of the propynyl radical.

Calculations were performed using the GAUSSIAN98 suite of programs [34] on a dual PIII-Xeon system and a dual 400 MHz IP30 SGI Octane system. Geometry optimizations and vibrational

frequency calculations were carried out as performed by Mebel [21]. Following an initial geometry optimization using B3LYP/6-311G(d,p), a subsequent optimization and frequency calculation was performed at the MP2/6-311G(d,p) level of theory, to ensure that the calculated ground state structure was stable. The vertical ionization potentials calculated using the UCCSD(T) method with 6-311G(d,p), cc-pVTZ, and aug-cc-pVTZ basis sets are presented in table 3. For consistency, no correction was made for the zero point energy. The highest level calculation yields a vertical IP of 10.75 eV to the CH_3CC^+ triplet state, consistent with the value of
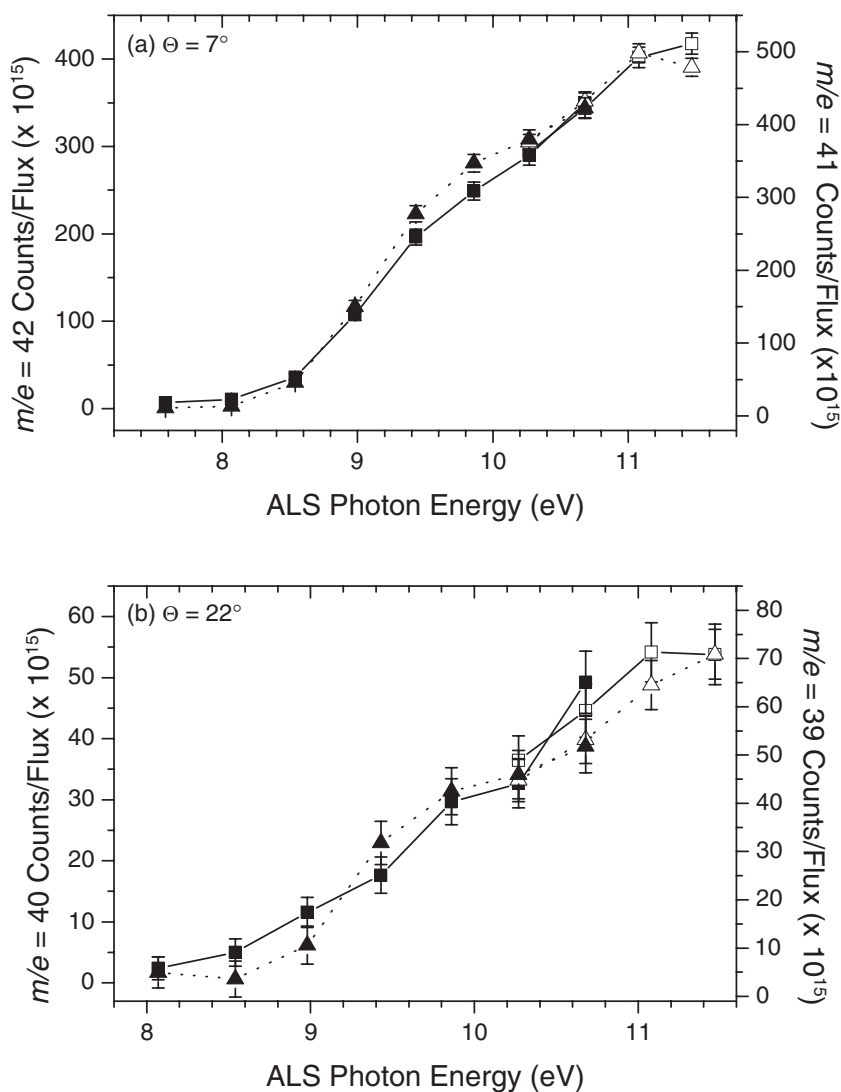
Figure 9. Photoionization efficiency curves for (a) $m/e = 42$ ($C_3D_3^+$) and $m/e = 41$ ($C_3D_2H^+$) photoproducts at $\Theta_{LAB} = 7°$ and for (b) $m/e = 40$ ($C_3D_2^+$) and $m/e = 39$ (C_3DH^+) at $\Theta_{LAB} = 22°$ from propyne-d₃ photodissociation. The solid squares and solid triangles represent the (a) $m/e = 42$ and $m/e = 41$ data points respectively and the (b) $m/e = 40$ and $m/e = 39$ data points respectively using the MgF₂ window for reduction of a residual high-energy tail in the undulator radiation. The unfilled squares and unfilled triangles represent the (a) $m/e = 42$ and $m/e = 41$ data points respectively and the (b) $m/e = 40$ and $m/e = 39$ data points respectively without using the MgF₂ window. The curves are scaled to one another for comparison. The data points are shown with 2σ error bars.

approximately 11 eV previously reported as an unpublished reference by Sun *et al.* [3]

4. Analysis

4.1 *Translational energy distributions*

In this section, centre-of-mass translational energy distributions used to fit the TOF spectra obtained on the two instruments are presented. It is considerably easier to fit the data obtained on the PI instrument, owing to greatly reduced dissociative ionization, so the procedure previously used in our analysis of

1,3-butadiene [2] was followed, in which distributions are fit to the PI data and then used to obtain branching ratios from the EI data.

The joint photofragment energy and angular distribution, $P(E_T, \theta)$, is given for each dissociation channel by

$$P(E_T, \theta) = P(E_T)\, T(\theta), \qquad (1)$$

where $P(E_T)$ and $T(\theta)$ are the uncoupled centre-of-mass translational energy and angular distributions, respectively. The excimer laser used in these experiments was not polarized. Thus, $T(\theta)$ will appear isotropic in the detection plane, given the rotating-source/fixed-detector
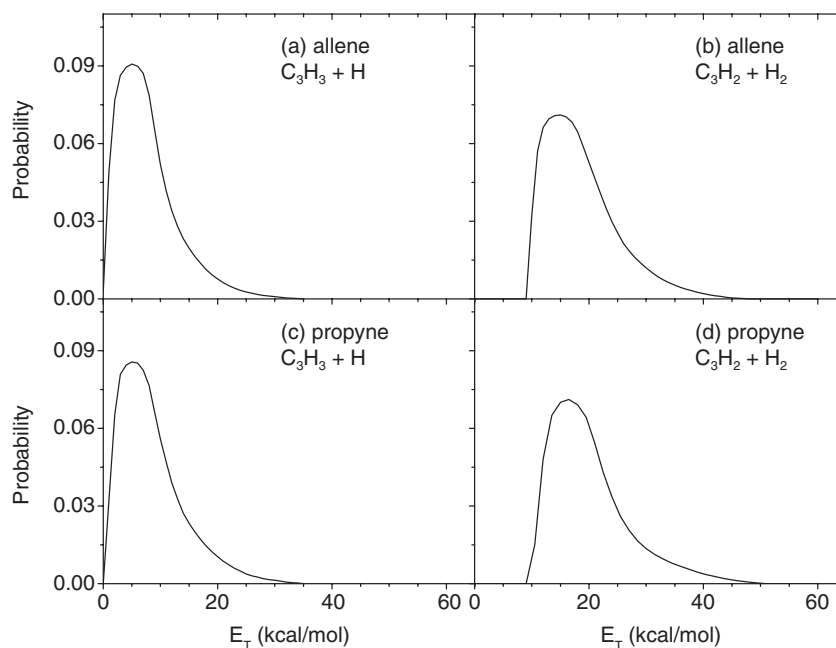
Figure 10. CM translational energy distribution for atomic hydrogen loss from (*a*) allene and (*c*) propyne dissociation. CM translational energy distribution for molecular hydrogen loss from (*b*) allene and (*d*) propyne dissociation.

geometry used on the PI instrument, where the direction of laser propagation is perpendicular to the plane defined by the molecular beam and the detector. The $P(E_T)$ distribution for each channel is determined through forward convolution, in which an assumed $P(E_T)$ distribution is convoluted over the various instrument parameters to simulate each of the TOF spectra. [35, 36] The $P(E_T)$ distributions are adjusted point-wise until the best simultaneous fit of the simulation to the TOF data at all observed angles is obtained.

Figure 10(*a*), (*b*) shows the $P(E_T)$ distributions used to fit the laboratory data for the allene photodissociation experiments, and figure 10(*c*), (*d*) shows the distributions used to fit the data from the propyne experiments. The contributions to the laboratory TOF data obtained from $P(E_T)$ distributions are shown in figures 2 and 3 (see captions for details). Figure 11 presents the $P(E_T)$ distributions used to fit the data from propyne-d_3 photodissociation; the same distributions were used to fit TOF spectra taken with either He or Ne as the carrier gas. There is an additional contribution to the propyne TOF data from photodissociation of a small amount of $(C_3H_4)_2$ present in the section of the propyne beam that was dissociated by the laser into two C_3H_4 fragments and appears as a dissociative ionization (DI) component in lower mass spectra; figure 12 shows the $P(E_T)$ distribution from propyne dimer dissociation used to fit this contribution. The calculated contributions of the $P(E_T)$ distributions for the various channels to the TOF spectra

are indicated in figures 2–5; details are given in the figure captions.

From figures 10 and 11, the $P(E_T)$ distributions for the atomic hydrogen loss channels are peaked near zero, while the $P(E_T)$ distributions for the molecular hydrogen loss channels are peaked well away from zero and extend more toward the energetic limit. The relevant quantities that can be extracted from the $P(E_T)$ distributions to characterize and compare them are listed in table 1, including the value of E_T at the peak of the distribution ($E_{T,peak}$), the maximum value of E_T in the distribution ($E_{T,max}$), the average translational energy release ($\langle E_T \rangle$), the maximum available energy for each channel (E_{avl}), and the fraction of available energy released into translation (f_T). The distributions for H-atom loss from allene and propyne are essentially identical, as are the distributions for H and D-atom loss from propyne-d_3. The distributions for H_2 loss from allene and propyne are also very similar. However, the values of E_{avl} and f_T in table 1 assume the identity of the C_3H_2 fragment be the three-center elimination product in each case, i.e. propadienylidene from allene and propargylene from propyne, a point covered further in the next section. The $P(E_T)$ distribution for D_2 loss from propyne-d_3 peaks at slightly lower E_T than that for HD loss. Energetics for deuterium-substituted propargylene are not available.

In figure 3, the TOF spectra for $m/e = 38$ at $\Theta_{LAB} = 10°$, taken at a photon energy of 11.7 eV, have a significant contribution from dissociative ionization of
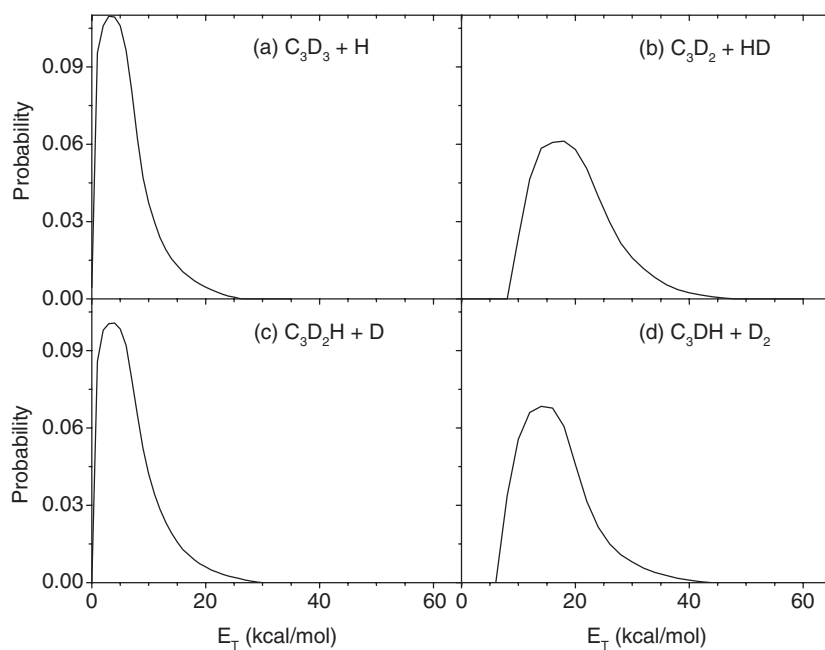
Figure 11. CM translational energy distributions for propyne-d$_3$ dissociation to produce (*a*) $C_3D_3 + H$, (*b*) $C_3D_2 + HD$, (*c*) $C_3D_2H + D$, and (*d*) $C_3DH + D_2$.
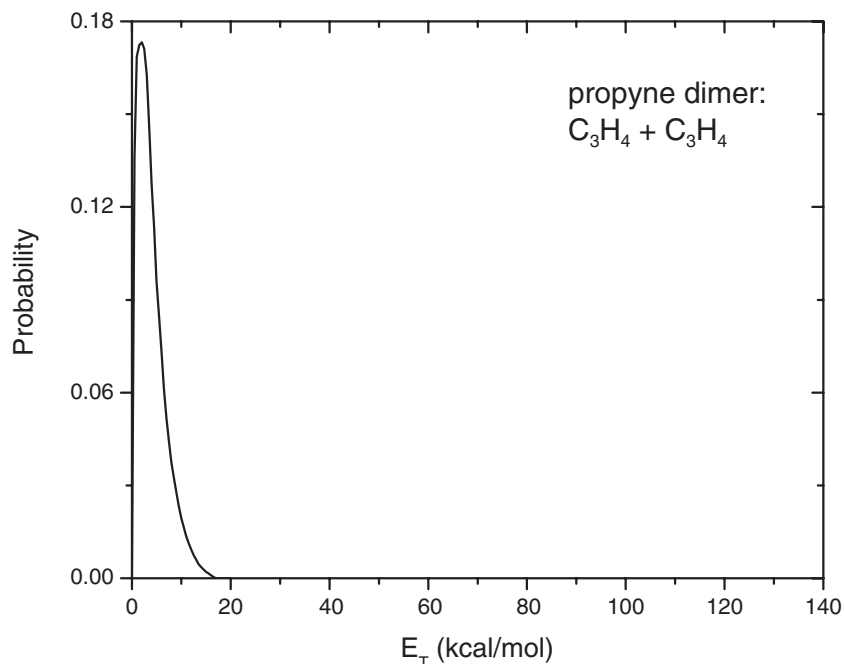
Figure 12. CM translational energy distribution for dimer dissociation in propyne photodissociation signal.

C_3H_3 products, but there is virtually no DI contribution at the larger scattering angle, $\Theta_{LAB} = 20°$, because of kinematic factors and the fact that the $P(E_T)$ distributions for H_2 loss peak at significantly higher translational energies. In figure 5, where results for HD and D_2 loss from propyne-d$_3$ are presented at $\Theta_{LAB} = 15°$, the contribution from DI is significantly lower at the lower photon energy, 9.5 eV, than at 11.5 eV. In our earlier paper [3], the DI contribution to the TOF spectra at $m/e = 38$ was incorrectly assigned to primary C_3H_2 signal for both allene and propyne photodissociation. As a result, the $P(E_T)$ distributions in that paper for the

Table 1. Relevant quantities characterizing CM translational energy distributions used to fit the laboratory frame data. Parameters are defined in text. All energies are in kcal/mol.

Channel	$E_{T,peak}$	$E_{T,max}$	$\langle E_T \rangle$	E_{avl}	f_T
allene R1: $C_3H_3 + H$	5	34	7.7	60.2[a]	0.13
propyne R1: $C_3H_3 + H$	5	34	8.5	58.5[a]	0.15
allene R2: $C_3H_2 + H_2$	15	48	18.7	65.0[a]	0.29
propyne R2: $C_3H_2 + H_2$	16.5	49.5	20.1	53.7[a]	0.37
propyne-d_3 R1: $C_3D_3 + H$	3	26	6.2	58.9[b]	0.11
propyne-d_3 R1: $C_3D_2H + D$	4	29	6.8	56.0[b]	0.12
propyne-d_3 R2: $C_3D_2 + HD$	18	46	19.9	–	–
propyne-d_3 R2: $C_3DH + D_2$	14	42	16.7	–	–

[a] Energies from [20] and [21].
[b] Energetics calculated in GAUSSIAN98 and described in the text.

$C_3H_2 + H_2$ channel were shifted toward very low translational energy, compared to those in figures 10 and 11. Thus, the extent of $C_3H_2 + H_2$ production was overestimated, resulting in an H:H$_2$ branching ratio that was too low.

Figures 6 and 7 show the fits to the EI TOF data using the $P(E_T)$ distributions in figures 10–12. The configuration of the EI instrument, in which the direction of laser propagation is in the plane defined by the molecular beam and the detector, allows for an anisotropic photofragment angular distribution to be used in the joint distribution, equation (1), but a satisfactory fit was obtained assuming an isotropic distribution. The TOF spectra in figure 6 from allene and propyne dissociation at $m/e = 39$ are relatively straightforward to fit, but those at $m/e = 38$ are dominated by dissociative ionization of mass 39 product and also have a significant contribution from DI of either allene or propyne dimer (the allene dimer $P(E_T)$, obtained by measuring TOF spectra at $m/e = 40$, is very similar to the propyne distribution in figure 12). Nonetheless, the various contributions to TOF spectra for $m/e = 38$ and lower mass ions can be determined, yielding branching ratios for H versus H$_2$ loss given below. In figure 7, only TOF spectra for H and D atom loss from propyne-d_3 are fitted and reported because the contributions from DI at the lower masses are too complex to sort out.

4.2 Intrachannel branching ratios

Product branching ratios for allene and propyne can be obtained from the PI TOF spectra only if relative photoionization cross sections are known for the various products. While our group has recently measured the absolute photoionization cross-section for the propargyl radical [37], cross-sections for the other species of interest (propynyl and the C_3H_2 products) are not known. Thus the EI data is used to extract branching ratios for H versus H$_2$ loss from allene and propyne. The same procedure is used as that employed for 1,3-butadiene [2] in which TOF spectra are measured at the parent ion m/e values and all ion masses where significant fragmentation from the parent ions occurs. Electron impact cross sections for the primary products are estimated using additivity rules [38] and result in cross sections of 6.56×10^{-16} cm^2 for C_3H_3 and 5.83×10^{-16} cm^2 for C_3H_2. These cross-sections, in conjunction with the fragmentation patterns, yield product branching ratios to within an accuracy of about 25%. Through this procedure, an H versus H$_2$ loss branching ratios of 90:10 was found for both allene and propyne photodissociation. The allene result agrees quite well with the ratio reported by Jackson *et al.* [5], whose experiments probed the H and H$_2$ fragments directly.

From the propyne-d_3 photodissociation experiments, intrachannel branching ratios can be obtained from the data for H loss versus D loss and for HD loss versus D$_2$ loss at different photoionization energies. These branching ratios can be obtained from the signal levels in the laboratory TOF spectra, following normalization by VUV intensity and number of laser shots. The fitting program using to simulate the TOF spectra returns the relative weights of the $P(E_T)$ distributions needed to reproduce the relative signal intensities of the TOF spectra for each channel.

Branching ratios for H loss versus D loss from the photodissociation of propyne-d_3 at 193 nm using different photoionization energies, 9.5 and 11.5 eV, are presented in table 2, using $m/e = 42$ and 41 TOF spectra at $\Theta_{LAB} = 7°$ and $10°$. For these values, no correction has been made for absolute photoionization cross-sections for the heavy mass fragments. From the table, a product branching ratio for H loss to D loss of ~1:1 is obtained. The two photoionization energies were chosen to lie below and above our calculated vertical IP for propynyl radical. The value for the H:D branching ratio that was obtained using EI detection is ~1:1. Furthermore, branching ratios for HD loss versus D$_2$ loss are presented in table 2, using $m/e = 40$ and 39 TOF spectra at $\Theta_{LAB} = 10°$ and $15°$. From these values, one can see that the HD:D$_2$ branching ratio is larger at 11.5 eV than at 9.5 eV; these energies lie above and below the IP of propadienylidene, 10.43 eV. [23]

Table 2. H/D and HD/D$_2$ branching ratios for propyne-d$_3$ dissociation from fits to $m/e = 42$ and 41 TOF spectra at $\Theta_{LAB} = 7°$ and $10°$ and fits to $m/e = 40$ and 39 TOF spectra at $\Theta_{LAB} = 10°$ and $15°$; the electron impact H/D branching ratio for propyne-d$_3$ dissociation is from fits to $m/e = 42$ and 41 TOF spectra at $\Theta_{LAB} = 7°$ and $9°$.

Channel	Photoionization energy (eV)	Contribution	Per cent
$C_3D_3 + H$	9.5	0.97	49
$C_3D_2H + D$	9.5	1.00	51
$C_3D_3 + H$	11.5	1.01	50
$C_3D_2H + D$	11.5	1.00	50
$C_3D_2 + HD$	9.5	1.09	52
$C_3DH + D_2$	9.5	1.00	48
$C_3D_2 + HD$	11.5	1.50	60
$C_3DH + D_2$	11.5	1.00	40
$C_3D_3 + H$	Electron impact	1.00	48
$C_3D_2H + D$	Electron impact	1.07	52

5. Discussion

5.1 *Allene*

The allene photolysis results and analysis presented in this paper are in agreement with the main features of the earlier work by Jackson *et al.* [5] The major products arising from one photon absorption correspond to losing atomic and molecular hydrogen, and our $P(E_T)$ distributions for those two channels are similar to those obtained by Jackson. We see no evidence for the $CH_2 + C_2H_2$ channel observed by Ni *et al.* at 193 nm [8] (and by Harich *et al.* at 157 nm [9]), possibly reflecting poorer kinematics in our experiment for the detection of fragments where the masses are relatively close, compared to H or H$_2$ loss. The $P(E_T)$ distributions are consistent with internal conversion to the ground state followed by statistical decay to products. For H atom loss, the $P(E_T)$ distribution is concentrated at very low translational energy, consistent with ground state dissociation to two radical species ($C_3H_3 + H$), for which no barrier to the reverse reaction is expected. On the other hand, the distribution for the minor $C_3H_2 + H_2$ channel (figure 10(b)), which peaks well away from $E_T = 0$, is consistent with dissociation over an exit barrier, as expected for a molecular elimination channel.

The $P(E_T)$ distribution $C_3H_2 + H_2$ shows no intensity for $E_T < 9$ kcal/mol. This value is close to the calculated exit barrier height of 9.4 kcal/mol with respect to C_3H_2 (propadienylidene) + H$_2$ products [20] (see figure 1), consistent with a 'late' transition state in which the energy gained from passing over the barrier is

channelled almost exclusively into product translation rather than the internal degrees of freedom. The calculated transition state geometry for 1,1-H$_2$ elimination shows the geometry of the C_3H_2 moiety to be very similar to that calculated for the asymptotic C_3H_2 product, consistent with our experimental observations.

The PIE curve in figure 8(a) supports past assignments of the C_3H_3 species as the propargyl radical. The curve in figure 8(b) for C_3H_2 from allene rises sharply above 10 eV, but there is a significant tail, i.e. nonzero signal, extending below 9 eV. Chen and co-workers [23, 39] used VUV photoionization mass and photoelectron spectroscopy to determine adiabatic IPs for cyclopropenylidene and propadienylidene to be 9.15 ± 0.03 eV and 10.43 ± 0.02 eV, respectively. These values were compared to corrected additivity and scaled *ab initio* results. This group also predicted a value of 8.76 eV for the IP of triplet propargylene, which was supported by their experimental results [22]. The singlet-triplet splitting for propargylene was calculated to be 15.1 kcal/mol using B3LYP-DFT and 17.0 kcal/mol using CASPT2 [40] suggesting an IP of approximately 8 eV for singlet propargylene.

The clear rise in the PIE curve in figure 8(b) above 10 eV certainly suggests propadienylidene production, the expected molecular product via three-centre elimination from allene (see figure 1). The PIE signal below 10.4 eV may all be from vibrationally excited propadienylidene. However, it is also possible that some isomerization to propyne occurs, given that the isomerization barriers [18, 24, 25] are substantially lower than the photon energy and the barriers to dissociation. In this case, the favoured molecular elimination product would be (singlet) propargylene, which would exhibit PIE signal at lower photon energies. Cyclopropenylidene is the most stable C_3H_2 isomer, with a heat of formation calculated to be 13.5 kcal/mol lower than that of propadienylidene [21]. The calculated barrier to formation of this product from cyclopropene, an intermediate along the allene-propyne isomerization pathway, is 102 kcal/mol (with respect to propyne) [25], so it is an additional candidate as a primary photodissociation product, though less favourable than propadienylidene.

5.2 *Propyne*

Regardless of whether allene or propyne is photodissociated, the $P(E_T)$ distributions and PIE curves for the $m/e = 39$ products are very similar. In addition, for propyne dissociation, the same $P(E_T)$ distributions fit the experimental data for C_3H_3 production regardless of whether the photon energy was below or above the calculated vertical IP of propynyl. The $P(E_T)$

distribution for H loss from propyne extends beyond the energetic limit for propynyl+H production (i.e. 18 kcal/mol). Finally, the PIE curves for $m/e = 39$ in figure 8(a) are essentially the same. These comparisons suggest that the C_3H_3 species formed by H-atom loss from propyne is predominantly the propargyl radical, a conclusion also drawn by Qadiri *et al.* [12, 13] on the basis of H-atom time-of-flight measurements on allene and propyne at 193.3, 203.3, 209.0, and 213.3 nm. Such a result would be expected if electronically excited propyne were to undergo internal conversion to the ground state before dissociating, because cleavage of the much stronger acetylenic C–H bond would be highly unfavourable from the perspective of statistical ground state decay. The similarity between the $P(E_T)$ distributions for H atom loss from allene and propyne is consistent with similar energetics and reaction path topologies for H atom loss from both species. As shown in figure 1, the two relevant C–H bond dissociation energies for propargyl formation differ by less than 1 kcal/mol, and dissociation on the ground state in both cases proceeds without a reverse barrier.

These points of comparison are reasonably compelling, but do not rule out entirely the possibility that there is some production of propynyl from propyne. For example, because there is only 18 kcal/mol available to propynyl+H products, excited state dissociation to form this channel might result in a $P(E_T)$ distribution that is not so different than that for ground state dissociation to propargyl+H. Nonetheless, it appears that propargyl is the dominant product from H-atom loss. Further insight into H-atom loss is provided by the propyne-d3 results discussed in the following section.

Next, consider H_2 loss from propyne. As was the case for allene, this channel is relatively minor, and the $P(E_T)$ distribution peaks well away from zero. These results are largely consistent with ground state dissociation followed by internal conversion; H_2 loss is disfavoured by the tighter transition state associated with molecular elimination as opposed to bond fission, and the $P(E_T)$ distribution is consistent with dissociation over an exit barrier with respect to products. The identity of the C_3H_2 product is of considerable interest. Based on the energetics in figure 1, propargylene is anticipated to be the favoured C_3H_2 product from propyne, and propadienylidene to be the favoured product from allene. In figure 8(b), the larger signal below 10 eV at $m/e = 38$ from propyne compared to allene is consistent with this prediction. On the other hand, the H:H_2 branching ratios and $P(E_T)$ distributions for H_2 loss are the same for allene and propyne, even though the barrier heights for the two 1,1 elimination pathways are somewhat different (i.e. 7.3 kcal/mol higher for propargylene formation from propyne).

These results raise the issue of how much isomerization occurs between propyne and allene prior to dissociation, a point more directly addressed by the propyne-d$_3$ results. Several measurements of isomerization between allene and propyne have been reported at temperatures corresponding to considerably lower internal energies than used in this work [24, 25, 41–43].

5.3 *Propyne-d$_3$*

5.3.1 H-atom loss channel. The propyne-d$_3$ results allow the issues of dissociation mechanism and product identity to be probed in more detail. If there were a combination of excited and ground state dissociation producing propynyl and propargyl, respectively, then one would expect different PIE curves and $P(E_T)$ distributions for the $m/e = 42$ and 41 channels corresponding to H and D loss, respectively. Instead, no significant difference was found in either type of measurement. In particular, both mass channels are fit by essentially the same $P(E_T)$ distribution, regardless of whether Ne or He was used as a seed gas (with Ne, the results of which are not shown, we are more sensitive to slower products) or whether the VUV photon energy was at or above the calculated vertical IP of propynyl. In addition, the D:H branching ratio is approximately 1:1 at the two VUV photon energies. Moreover, using EI detection, the D:H branching ratio was also found to be ~1:1. Thus, it appears that H atom loss from propyne-d$_3$ does not result from excited state dissociation to $CD_3CC + H$.

The results then raise the issue of why H atom loss is observed at all from propyne-d$_3$, and, more specifically, why the D:H branching ratio is approximately 1:1, because statistical decay of ground state CD_3CCH formed by internal conversion should result in D atom loss only. H atom loss can only occur through isotopic scrambling on the ground state prior to dissociation, either through isomerization to cyclopropene and back to propyne, resulting in CD_2HCCD, which could then lose an H atom to form propargyl-d$_3$, or by isomerization to allene-d$_3$, CD_2CCDH, in which all D and H atoms are chemically equivalent. The maximum calculated barrier height [18, 25] along the isomerization pathway from propyne to cyclopropene is 61 kcal/mol, while that for isomerization from cyclopropene to allene is 66 kcal/mol, so these scrambling processes are energetically accessible subsequent to internal conversion. Evidence for scrambling in propyne was also seen at 157 nm excitation [10].

If isotopic scrambling of propyne-d3 were complete prior to dissociation, then there would be three times as much CD_2HCCD as CD_3CCH. Moreover, if only dissociation to propargyl occurred from C–H(D)

Table 3. Results from vertical ionization potential calculations (in units of eV) for the propynyl radical optimized using MP2/6-311G(d,p) following B3LYP/6-311G(d,p).

Species	UCCSD(T) 6-311G(d,p)	UCCSD(T) cc-pVTZ	UCCSD(T) aug-cc-pVTZ
CH_3CC^+ (singlet)	13.12	13.23	13.26
CH_3CC^+ (triplet)	10.57	10.71	10.75
CH_3CC (neutral)	0	0	0

Table 4. Vibrational frequencies (in units of cm^{-1}) for deuterated propargyl radicals, scaled as mentioned in the text.

CD_2CCD	CHDCCD	CD_2CCH
304.92	318.87	317.77
334.54	340.97	379.97
407.14	416.35	477.04
493.64	494.26	562.72
562.32	626.77	631.15
832.48	861.95	833.92
926.28	1052.88	934.35
1170.46	1318.08	1179.82
1891.98	1893.71	1985.75
2253.90	2313.30	2254.04
2379.29	2611.07	2379.30
2433.05	3153.15	3417.01

Table 5. Densities of states for deuterated propargyl radicals produced by propyne-d3 dissociation.

Reaction products	Beyer–Swinehart	Whitten–Rabinovich
$CD_2CCD + H$	1.28×10^9	1.34×10^9
$CHDCCD + D$	4.65×10^8	4.71×10^8
$CD_2CCH + D$	4.10×10^8	4.15×10^8

cleavage on the methyl group, then one would expect, at first glance, a D:H branching ratio of 3.3:1 rather than 1:1. However, assuming that both D and H loss are statistical with no exit barriers, RRKM theory predicts the branching ratio will also be influenced by the sum of vibrational states available to the various propargyl isotopomers for dissociation at 193 nm, which, in turn, depend on their zero point energies and vibrational frequencies. Each possible deuterated propargyl product from the dissociation of propyne-d₃ (or allene-d₃) was considered, i.e. CD_2CCH, $CDHCCD$, and CD_2CCD. Vibrational frequencies and zero point vibrational energy (ZPVE) corrections were determined using the GAUSSIAN98 suite of programs [34] on a dual Intel PIII-Xeon system. Vibrational frequencies were scaled based on the recommendations of Bauschlicher and Partridge [44]. Structures were optimized at the

B3LYP/6-311G(d,p) level of theory and vibrational frequency calculations were carried out at B3LYP/6-311+ G(3df,2p). For this basis set and method, vibrational frequencies were scaled by 0.989, and these scaled frequencies were used to calculate the ZPVE correction. The state sums were calculated using the Beyer–Swinehart algorithm for direct count of vibrational states [45, 46] and the Whitten–Rabinovich method [47]. A bin width of $1 cm^{-1}$ was used for the sum of states direct count calculation.

The calculated vibrational frequencies are shown in table 4. Calculations for propyne and propyne-d₃ yielded a difference in ZPVE of 5.83 kcal/mol, and calculations for the propargyl radical (CH_2CCH) yielded differences in ZPVE of 3.50 kcal/mol (CD_2CCH), 3.43 kcal/mol (CDHCCD), and 5.45 kcal/mol (CD_2CCD). Thus, the energy available following 193 nm photolysis to produce propargyl radical and a hydrogen atom would be $20\,746.4\,cm^{-1}$ for propyne and $19\,620.3\,cm^{-1}$ ($CD_2CCH + D$), $19\,596.1\,cm^{-1}$ (CDHCCD + D), and $20\,612.7\,cm^{-1}$ ($CD_2CCD + H$) for propyne-d₃. Table 5 shows the densities of states for the possible reactions to form propargyl radical and atomic hydrogen or deuterium. At these energies, the density of states for $CD_2CCD + H$ is three times that for either CHDCCD + D or $CD_2CCH + D$, thereby almost exactly compensating for the 3.3:1 D:H ratio expected without considering product densities of states. It thus appears that isotopic scrambling of the hydrogen atoms on propyne competes effectively with H atom loss. The question remains, however, as to whether H atom scrambling results in significant allene population prior to dissociation. This point is considered in the next section.

5.3.2 H₂ loss channel. The H₂ loss channel for propyne-d₃ offers further insights into the competition between dissociation and isotopic scrambling. According to figure 1, if no isomerization were to occur, then molecular hydrogen elimination from propyne-d₃ would result solely in $D_2 + DCCCH$ production via a three-center transition state; production of $HD + CCCD_2$ through a five-centre transition state [21] involves passage over a considerably higher barrier. However, as shown in table 2, HD:D₂ branching ratios are observed to be between 1:1 and 1.5:1, depending on the photon energy, implying again that there is significant isotopic scrambling in propyne-d₃ prior to molecular hydrogen loss. The question then arises as to the identity of the C₃HD and C₃D₂ fragments, and the related issue of whether this channel comes exclusively from propyne or from a mixture of propyne, cyclopropene, and allene.

The $P(E_T)$ distributions for HD versus D₂ loss in figure 11 are similar but not identical, with slightly more product translational energy seen for HD loss. On the

other hand, the PIE curves in figure 9(*b*) are identical within their error bars, indicating no difference between the C_3HD and C_3D_2 fragments. Moreover, these curves are more similar to the PIE curve H_2 loss from propyne than the corresponding curve for H_2 loss from allene, with all three propyne PIE curves showing more signal below 10 eV. Taken together, it appears that the HD and D_2 loss channels are very similar, and that, overall, there is a preference for forming C_3H_2 species with lower IP's from propyne (i.e. propargylene and cyclopropadienylidene) than from allene.

The last conclusion is particularly important, as it represents the only real evidence that isotopic scrambling is not so rapid as to completely eliminate any differences between the photodissociation of allene and propyne. However, given the relatively large error bars on the PIE curves for H_2 elimination, this conclusion is tentative and in need of further experimental confirmation, perhaps by performing state-resolved measurements on the H_2 fragment from allene, propyne, and propyne-d$_3$.

6. Conclusions

Allene, propyne, and propyne-d$_3$ have been photodissociated at 193 nm under collisionless conditions, and the photoproducts have been probed via the technique of photofragment translational spectroscopy coupled with both tunable VUV and electron impact ionization detection. Each species shows atomic and molecular hydrogen (or deuterated analogues thereof) elimination channels, with molecular hydrogen a minor channel (~10%) for allene and propyne. Product $P(E_T)$ distributions are very similar for atomic or molecular loss channels, independent of precursor, and are consistent with a dissociation mechanism dominated by internal conversion to the ground state prior to dissociation. The $P(E_T)$ distributions for H atom loss peak at very low translational energy (<5 kcal/mol), while those for H_2 loss show considerably greater translational energy release, consistent with passage over a barrier with respect to products.

Photoionization efficiency (PIE) curves for H atom loss from allene and propyne are essentially identical, indicating the C_3H_3 product is primarily the propargyl radical in both cases. In addition, the PIE curves for H and D atom loss from propyne-d$_3$ were found to be identical, and the branching ratio for H:D loss to be approximately unity. These results show that extensive isotopic scrambling occurs prior to dissociation, and that loss of either an H or a D atom produces the propargyl radical; if any propynyl radical is produced following loss of an H atom, then it is a relatively

insignificant process. The extensive isotopic scrambling must occur either through a cyclopropene intermediate or by (reversible) formation of allene.

If substantial isomerization between allene and propyne does occur prior to dissociation, one would expect the photodissociation dynamics of the two molecules to be indistinguishable, and indeed, the $P(E_T)$ distributions and H:H_2 branching ratios are largely independent of parent compound. On the other hand, the PIE curves for C_3H_2 products from allene and propyne differ enough to suggest identifying the dominant isomers as propadienylidene and (singlet) propargylene, respectively; the PIE curves for C_3HD and C_3D_2 from propyne-d$_3$ are very similar to one another and to the PIE curve for C_3H_2 from propyne. Taken together, these PIE curves offer the only evidence of differences between the photodissociation dynamics of allene and propyne, suggesting that isomerization between allene and propyne is not complete prior to dissociation. However, this observation must be regarded quite tentatively, owing to the relatively low signal levels for molecular hydrogen loss from all precursors.

References

[1] J.C. Robinson, W.Z. Sun, S.A. Harris, F. Qi, D.M. Neumark. *J. chem. Phys.*, **115,** 8359 (2001).
[2] J.C. Robinson, S.A. Harris, W.Z. Sun, N.E. Sveum, D.M. Neumark. *J. Am. chem. Soc.*, **124,** 10211 (2002).
[3] W. Sun, K. Yokoyama, J.C. Robinson, A.G. Suits, D.M. Neumark. *J. chem. Phys.*, **110,** 4363 (1999).
[4] S. Satyapal, R. Bersohn. *J. phys. chem.*, **95,** 8004 (1991).
[5] W.M. Jackson, D.S. Anex, R.E. Continetti, B.A. Balko, Y.T. Lee. *J. chem. Phys.*, **95,** 7327 (1991).
[6] K. Seki, H. Okabe. *J. phys. Chem.*, **96,** 3345 (1992).
[7] X. Song, Y. Bao, R.S. Urdahl, J.N. Gosine, W.M. Jackson. *Chem. Phys. Lett.*, **217,** 216 (1994).
[8] C.-K. Ni, J.D. Huang, Y.T. Chen, A.H. Kung, W.M. Jackson. *J. chem. Phys*, **110,** 3320 (1999).
[9] S. Harich, Y.T. Lee, X. Yang. *Phys. Chem. Chem. Phys.*, **2,** 1187 (2000).
[10] S. Harich, J.J. Lin, Y.T. Lee, X. Yang. *J. chem. Phys.*, **112,** 6656 (2000).

[11] X. Chen, Y. Ganot, I. Bar, S. Rosenwaks. *J. chem. Phys.*, **113**, 5134 (2000).

[12] R.H. Qadiri, E.J. Feltham, E.E.H. Cotrill, N. Taniguchi, M.N.R. Ashfold. *J. chem. Phys.*, **116**, 906 (2002).

[13] R.H. Qadiri, E.J. Feltham, N.H. Nahler, R.P. Garcia, M.N.R. Ashfold. *J. chem. Phys.*, **119**, 12842 (2003).

[14] H.F. Bettinger, P.R. Schreiner, P.v.R. Schleyer, H.F.I. Schaefer. *J. phys. Chem.*, **100**, 16147 (1996).

[15] N. Honjou, J. Pacansky, M. Yoshimine. *J. Am. chem. Soc.*, **106**, 5361 (1984).

[16] N. Honjou, J. Pacansky, M. Yoshimine. *J. Am. chem. Soc.*, **107**, 5332 (1985).

[17] M. Yoshimine, J. Pacansky, N. Honjou. *J. Am. chem. Soc.*, **111**, 2789 (1989).

[18] M. Yoshimine, J. Pacansky, N. Honjou. *J. Am. chem. Soc.*, **111**, 4198 (1989).

[19] C.W.J. Bauschlicher, S.R. Langhoff. *Chem. Phys. Lett.*, **193**, 380 (1992).

[20] W.M. Jackson, A.M. Mebel, S.H. Lin, Y.T. Lee. *J. phys. Chem. A*, **101**, 6638 (1997).

[21] A.M. Mebel, W.M. Jackson, A.H.H. Chung, S.H. Lin. *J. Am. chem. Soc.*, **120**, 5751 (1998).

[22] T. Gilbert, R. Pfab, I. Fischer, P. Chen. *J. chem. Phys.*, **112**, 2575 (2000).

[23] H. Clauberg, D.W. Minsek, P. Chen. *J. Am. chem. Soc.*, **114**, 99 (1992).

[24] S.G. Davis, C.K. Law, H. Wang. *J. phys. Chem. A*, **103**, 5889 (1999).

[25] J.H. Kiefer, P.S. Mudipalli, S.S. Sidhu, R.D. Kern, B.S. Jursic, K. Xie, H. Chen. *J. phys. Chem. A*, **101**, 4057 (1997).

[26] D.A. Blank. Molecular beam studies of unimolecular and bimolecular chemical reaction dynamics using VUV synchrotron radiation as a product probe. PhD thesis, University of California, Berkeley, (1997).

[27] X. Yang, D.A. Blank, J. Lin, A.M. Wodtke, A.G. Suits, Y.T. Lee. *Rev. Sci. Instrum.*, **68**, 3317 (1997).

[28] P.A. Heimann, M. Koike, C.W. Hsu, M. Evans, C.Y. Ng, D. Blank, X.M. Yang, C. Flaim, A.G. Suits, Y.T. Lee. Performance of the vuv high resolution and high flux beamline for chemical dynamics studies at the advanced light source, SPIE Proc., 1996.

[29] M. Koike, P.A. Heimann, A.H. Kung, T. Namioka, R. Digennaro, B. Gee, N. Yu. *Nucl. Instrum. Meth. Phys. Res. A*, **347**, 282 (1994).

[30] A.G. Suits, P. Heimann, X.M. Yang, M. Evans, C.W. Hsu, K.T. Lu, Y.T. Lee, A.H. Kung. *Rev. Sci. Instrum.*, **66**, 4841 (1995).

[31] Y.T. Lee, J.D. McDonald, P.R. LeBreton, D.R. Herschbach. *Rev. Sci. Instrum.*, **40**, 1402 (1969).

[32] S.G. Lias, J.E. Bartmas, J.F. Liebman, J.L. Holmes, R.D. Levin, W.G. Mallard. *J. phys. Chem. Ref. Data*, **117**, (1988).

[33] D.W. Minsek, P. Chen. *J. phys. Chem.*, **94**, 8399 (1990).

[34] M.J. Frisch, G.W. Trucks, H.B. Schlegel, G.E. Scuseria, M.A. Robb, J.R. Cheeseman, V.G. Zakrzewski, J.A. Montgomery, R.E. Stratmann, J.C. Burant, S. Dapprich, J.M. Millam, A.D. Daniels, K.N. Kudin, M.C. Strain, O. Farkas, J. Tomasi, V. Barone, M. Cossi, R. Cammi, B. Menucci, C. Pomelli, C. Adamo, S. Clifford, J. Ochterski, G.A. Petersson, P.Y. Ayala, Q. Cui, K. Morokuma, D.K. Malick, A.D. Rabuck, K. Raghavachari, J.B. Foresman, J. Cioslowski, J.V. Oritz, A.G. Baboul, B.B. Stefanov, G. Liu, A. Liashenki, P. Piskorz, I. Komaromi, R. Gomperts, R.L. Martin, D.J. Fox, T. Keith, M.A. Al-Laham, C.Y. Peng, A. Nanayakkara, M. Challacombe, P.M.W. Gill, B. Johnson, W. Chen, M.W. Wong, J.L. Andres, C. Gonzalez, M. Head-Gordon, E.S. Replogle, J.A. Pople, GAUSSIAN 98; Revison A.9 edn, Gaussian, Inc., Pittsburgh, PA, (1998).

[35] X. Zhao. PhD thesis, University of California, Berkeley (1988).

[36] J.D. Myers. PhD thesis, University of California, Berkeley (1993).

[37] J.C. Robinson, N.E. Sveum, D.M. Neumark. *J. chem. Phys.*, **119**, 5311 (2003).

[38] A.M. Schmoltner. PhD thesis, University of California, Berkeley (1989).

[39] J.A. Blush, H. Clauberg, D.W. Kohn, D.W. Minsek, X. Zhang, P. Chen. *Accts. Chem. Res.*, **25**, 385 (1992).

[40] L. Vereecken, K. Pierloot, J. Peeters. *J. chem. Phys.*, **108**, 1068 (1998).

[41] M. Karni, I. Oref, S. Barzilaigilboa, A. Lifshitz. *J. phys. Chem.*, **92**, 6924 (1988).

[42] T. Kakumoto, T. Ushirogouchi, K. Saito, A. Imamura. *J. phys. Chem.*, **91**, 183 (1987).

[43] J.H. Kiefer, S.S. Kumaran, P.S. Mudipalli. *Chem. Phys. Lett.*, **224**, 51 (1994).

[44] C.W.J. Bauschlicher, H. Partridge. *J. chem. Phys.*, **103**, 1788 (1995).

[45] T. Baer, W.L. Hase. *Unimolecular Reaction Dynamics: Theory and Experiments*, Oxford University Press, New York (1996).

[46] R.G. Gilbert, S.C. Smith. *Theory of Unimolecular and Recombination Reactions*, 1st edn, Blackwell Scientific, Cambridge, MA (1990).

[47] J.I. Steinfeld, J.S. Francisco, W.L. Hase. *Chemical Kinetics and Dynamics,* Prentice-Hall, Engelwood Cliffs, NJ (1989).